Interaction of an Engineered [3Fe-4S] Cluster with a Menaquinol Binding Site of *Escherichia coli* DMSO Reductase†

Richard A. Rothery and Joel H. Weiner*

MRC Group in the Molecular Biology of Membranes, Department of Biochemistry, 474 Medical Sciences Building, University of Alberta, Edmonton, Alberta, Canada T6G 2H7

Received July 12, 1995; Revised Manuscript Received November 27, 1995⊗

ABSTRACT: We have characterized by EPR the interaction of the $E_{m,7} = -50$ mV [4Fe-4S] cluster of *Escherichia coli* DMSO reductase (DmsABC) with a menaquinol (MQH_2) binding site. Potentiometric titrations indicate that in DmsAB^{C102S}C, the $E_{m,7} = -50$ mV [4Fe-4S] cluster is replaced by an $E_{m,7} = +260$ mV [3Fe-4S] cluster. The Q-pool coupling assay in combination with the MQH_2 analog HOQNO (2-*n*-heptyl-4-hydroxyquinoline-*N*-oxide) was used to examine the effect of the DmsB^{C102S} mutation on physiological electron transfer through DmsABC. Forward electron transfer through the mutant (MQH_2 to DmsA) is blocked in the Q-pool coupling assay, but reverse electron transfer (DmsA to MQ) is not. HOQNO elicits a significant change in the EPR line shape of the oxidized DmsAB^{C102S}C [3Fe-4S] cluster but has no effect on the line shape of the reduced [4Fe-4S] clusters. We have identified a residue in DmsC involved in MQH_2 oxidation, DmsC^{H65}, and in a double mutant, DmsAB^{C102S}C^{H65R}, the DmsC mutation blocks the HOQNO effect on the [3Fe-4S] EPR line shape, suggesting that the DmsC^{H65R} mutation either blocks HOQNO binding or blocks a conformational link between a HOQNO binding site and the DmsB^{C102S} [3Fe-4S] cluster. These results suggest that the MQH_2 binding site of DmsC is conformationally and functionally linked to the $E_{m,7} = -50$ mV [4Fe-4S] cluster of DmsB.

Escherichia coli, when grown anaerobically with dimethyl sufoxide (DMSO)[1] as respiratory oxidant, develops a respiratory chain terminated by a membrane-bound menaquinol: DMSO oxidoreductase (DMSO reductase, DmsABC) (Weiner *et al*., 1992). The operon encoding DmsABC (*dmsABC*) has been cloned (Bilous & Weiner, 1988) and sequenced (Bilous *et al*., 1988), and the enzyme it encodes has been purified to homogeneity (Weiner *et al*., 1988). DmsABC is a heterotrimer comprising a molybdenum cofactor containing catalytic subunit (DmsA, 87.4 kDa), an [Fe-S] cluster containing electron-transfer subunit (DmsB, 23.1 kDa), and a membrane-intrinsic anchor subunit (DmsC, 30.8 kDa) (Bilous *et al.*, 1988). DmsA and DmsB comprise a cytoplasmically localized catalytic dimer (Rothery & Weiner, 1993; Sambasivarao *et al*., 1990) anchored to the cytoplasmic membrane by DmsC (Weiner *et al*., 1993). The enzyme can be readily overexpressed in cells harboring plasmids bearing the *dmsABC* operon, and the overexpressed enzyme assembles normally into the cytoplasmic membrane (Cammack & Weiner, 1990; Weiner *et al.*, 1988). DmsABC is a good model system for a group of complex iron−sulfur molybdoenzymes including *E. coli* formate dehydrogenase (FdnGHI) (Berg *et al.*, 1991), the two *E. coli* nitrate reductases (NarGHJI and NarZYWV) (Blasco *et al.*, 1989, 1990), and *Wollinella succinogenes* polysulfide reductase (PsrABC) (Krafft *et al*., 1992).

DmsABC contains four [4Fe-4S] clusters (Cammack & Weiner, 1990) with midpoint potentials ($E_{m,7}$'s) of −50, −120, −240, and −330 mV. Ligands to these four [4Fe-4S] clusters are provided by 16 Cys residues in DmsB which are arranged in four groups (I−IV) with sequences similar to the Cys groups ligating the [4Fe-4S] clusters of many bacterial ferredoxins (Bruschi & Guerlesquin, 1988) and respiratory chain enzymes ($C_AX_2C_BX_{2-11}C_CX_3C_DP$) (Weiner *et al.*, 1992). The Cys groups of DmsB are similar to those of the electron-transfer subunits of the two *E. coli* nitrate reductases NarGHI (NarH) (Blasco *et al.*, 1989) and NarZYV (NarY) (Blasco *et al.*, 1990). The two nitrate reductases contain three [4Fe-4S] clusters and one [3Fe-4S] cluster (Guigliarelli *et al.*, 1992; Johnson *et al.*, 1985a), and this difference in [Fe-S] cluster composition can be explained by the presence of a Trp residue at the C_B position of Cys group III of NarH and NarY. By changing the C_B residue of DmsB Cys group III to a Trp or Ser, we have been able to alter the [Fe-S] cluster composition of DmsABC to make it equivalent to that of the two nitrate reductases (Rothery & Weiner, 1991). These mutant enzymes, DmsAB^{C102S}C and DmsAB^{C102W}C, are unable to oxidize menaquinol (MQH_2, $E_{m,7} = -70$ mV) and are therefore unable to support growth with DMSO ($E_{m,7} = +160$ mV) as respiratory oxidant.

In order to fully interpret the effect of the mutations of Cys group III C_B, it is essential to determine which of the potentiometrically identified [4Fe-4S] clusters is replaced by a [3Fe-4S] cluster in the mutant enzymes. Similar cluster interconversions have recently been reported for the F_X and F_A [4Fe-4S] clusters of photosystem I of *Synechococcus* sp. PC 6301 (Warren *et al.*, 1993; Zhao *et al.*, 1992). The F_A

† This work was funded by a grant from the Medical Research Council of Canada to J.H.W. (PG11440).

* Author to whom correspondence should be addressed. Telephone: (403) 492-2761. Electronic mail address: joel.weiner@ualberta.ca.

⊗ Abstract published in *Advance ACS Abstracts*, February 15, 1996.

[1] Abbreviations: DmsABC, DMSO reductase; DMSO, dimethyl sulfoxide; FrdABCD, fumarate reductase; GF, glycerol−fumarate minimal medium; HOQNO, 2-*n*-heptyl-4-hydroxyquinoline-*N*-oxide; MQH_2, menaquinol; MQ, menaquinone; NarGHI, nitrate reductase A; TMAO, trimethylamine-*N*-oxide.

0006-2960/96/0435-3247$12.00/0

Table 1: Bacterial Strains and Plasmids

strain or plasmid	description	source
E. coli strains		
HB101	*supE*44 *hsdS*20 (r_B^- m_B^-) *recA*13 *ara*-14 *proA*2 *lacY*1 *galK*2 *rpsL*20 *xyl*-5 *mtl*-1	lab collection
DSS301	*supE hsd*Δ5 *thi* Δ(*lac-proAB*) *F′* [*traD*36 *proAB*$^+$ *lacI*q *lacZ*Δ′15] Kan^R Δ*dmsABC*	Sambasivarao and Weiner (1991)
F36	HB101 (DmsABC molybdenum cofactor insertion mutant)[a]	Cammack and Weiner (1990)
plasmids		
pBR322	Tet^R Amp^R	Pharmacia
pDMS160	pBR322 Amp^R (*dmsABC*)$^+$	Rothery and Weiner (1991)
pDMS160-C102S	pBR322 Amp^R (*dmsAB*^{C102S}*C*)$^+$	Rothery and Weiner (1991)
pDMS160-C102W	pBR322 Amp^R (*dmsAB*^{C102W}*C*)$^+$	Rothery and Weiner (1991)
pDMS160-H65R	pBR322 Amp^R (*dmsABC*^{H65R})$^+$	this study
pDMS160-C102S-H65R	pBR322 Amp^R (*dmsAB*^{C102S}*C*^{H65R})$^+$	this study
pDMS160-C102W-H65R	pBR322 Amp^R (*dmsAB*^{C102W}*C*^{H65R})$^+$	this study

[a] *E. coli* F36 is deficient in molybdenum cofactor insertion into DmsABC.

cluster is ligated by a 2[4Fe-4S] ferredoxin-type protein (PsaC) which contains two Cys groups (I and II). By changing the C_B of both groups to Asp, it was found that F_A is ligated by Cys group II and can be changed to a [3Fe-4S] cluster (Zhao *et al.*, 1992). The F_X cluster of photosystem I is not ligated by a typical ferredoxin-like Cys group. However, by changing C565 of PsaB to Ser, it was possible to partially convert the population of F_X to a [3Fe-4S] cluster (Warren *et al.*, 1993). In *E. coli* fumarate reductase (FrdABCD), it has been possible to change the [3Fe-4S] FR3 cluster to a [4Fe-4S] cluster by changing the Val residue at the C_B position of the third Cys group of FrdB to a Cys (V207C) (Manadori *et al.*, 1992).

We recently applied the technique of distance estimations using the exogenous paramagnetic probe dysprosium(III) complexed with EDTA (DyEDTA) to study the location of the [3Fe-4S] cluster in DmsAB^{C102S}C (Rothery & Weiner, 1993). This cluster appears to be located approximately 21 Å below the cytoplasmic side surface of the DmsABC holoenzyme, close to the cytoplasmic side membrane surface level. This position is consistent with a role for the wild-type [4Fe-4S] cluster to which Cys group III provides ligands in electron transfer from MQH_2. In the mitochondrial cytochrome bc_1 complex (complex III), the Q_o site is located close to the Rieske [2Fe-2S] cluster (Ding *et al.*, 1992; Ohnishi *et al.*, 1994; Robertson *et al.*, 1990; Trumpower, 1990). Some of the evidence for this has come from the use of ubiquinol analogs which both inhibit the ubiquinol: cytochrome *c* oxidoreductase activity of the complex and significantly perturb the EPR line shape and redox properties of the Rieske center (Robertson *et al.*, 1990; von Jagow & Ohnishi, 1985). The interaction of the MQH_2 analog HOQNO (2-*n*-heptyl-4-hydroxyquinoline-*N*-oxide) with the succinate:menaquinone oxidoreductase of *Bacillus subtilis* has recently been studied. In this case, the inhibitor binds to the enzyme, perturbing the optical and redox properties of the low potential heme *b* (Smirnova *et al.*, 1995), but has no effect on the EPR properties of the [3Fe-4S] cluster, S3 (Hägerhäll *et al.*, 1995). It would therefore be interesting to examine the effect of a MQH_2 analog on the EPR properties of the [3Fe-4S] clusters of DmsAB^{C102S}C and DmsAB^{C102W}C to determine if they are in close proximity to, or conformationally linked to, the MQH_2 binding sites of their respective mutant enzymes.

In this paper, we describe the potentiometric characterization of the [Fe-S] clusters of DmsAB^{C102S}C and DmsAB^{C102W}C which each contain a genetically engineered [3Fe-4S] cluster. We have investigated the effect of these mutations on the electron flow through DmsABC using the Q-pool coupling assay (Trieber *et al.*, 1994) and demonstrate the interaction of the [3Fe-4S] clusters in the two mutants with a MQH_2 binding site of DmsABC. We have also identified an amino acid residue in DmsC which appears to be important in defining a MQH_2 binding site of DmsABC.

MATERIALS AND METHODS

Bacterial Strains and Plasmids. The *E. coli* strains and plasmids used in this study are listed in Table 1. Studies of the expression and function of mutant and wild-type DmsABC were carried out with *E. coli* HB101 and DSS301 (Sambasivarao & Weiner, 1991). Potentiometric redox titrations were carried out using *E. coli* F36 (Cammack & Weiner, 1990), a mutant which does not assemble the molybdenum cofactor into DmsABC.

Oligonucleotide-Directed Mutagenesis of DmsC. Oligonucleotide-directed mutagenesis was carried out as previously described (Rothery & Weiner, 1991; Trieber *et al.*, 1994). H65 of DmsC was changed to an Arg residue (a codon change of CAT to CGT) to mimic an equivalent mutation (H82R) in the FrdC subunit of *E. coli* fumarate reductase (FrdABCD) (Weiner *et al.*, 1986). Plasmids bearing double mutations of DmsB and DmsC were created by subcloning a 1.08 kbp *Sst*I−*Sal*I fragment bearing *dmsC*^{H65R} from pDMS160-H65R into pDMS160-C102S and pDMS160-C102W to create pDMS160-C102S-H65R and pDMS160-C102W-H65R, respectively. All manipulations of plasmids and strains were carried out as previously described (Sambrook *et al.*, 1989).

Growth of Cells. To assess the ability of the mutants to support growth, DSS301 cells transformed with the mutant plasmids were grown anaerobically at 37 °C on a glycerol−DMSO minimal medium (Bilous & Weiner, 1985). For detailed biochemical and EPR studies, DSS301, HB101, and F36 transformed with the mutant plasmids were grown in 20 L batch cultures at 37 °C on a glycerol−fumarate minimal medium (Condon & Weiner, 1988) for 24, 48, and 48 h, respectively. This medium has been shown to result in the highest levels of expression and assembly of DmsABC into the cytoplasmic membrane (Bilous & Weiner, 1988). Where appropriate, ampicillin (100 μg mL^{-1}), streptomycin (100 μg mL^{-1}), and kanamycin (50 μg mL^{-1}) were included in the growth media.

Preparation of Membrane Vesicles. Cells were harvested and washed, and membranes were prepared by French pressure cell lysis and differential centrifugation (Rothery

& Weiner, 1991) in 50 mM MOPS, 70 mM TMAO, and 5 mM EDTA (pH 7.0). The buffer used during the French pressing step contained 0.2 mM PMSF. Prior to the preparation of EPR samples, the buffer was exchanged for 100 mM MOPS and 5 mM EDTA (pH 7.0). TMAO-dependent oxidation of reduced benzyl viologen ($BV^{\bullet+}$) by membrane preparations was determined as previously described (Cammack & Weiner, 1990).

Redox Potentiometry. Redox titrations were carried out at 25 °C under argon in an anaerobic chamber (Dutton, 1978) equipped with an anaerobic transfer chamber (Chamorovsky & Cammack, 1982). Membranes containing overexpressed wild-type and mutant DmsABC were suspended in 100 mM MOPS and 5 mM EDTA (pH 7.0) and were transferred to the anaerobic chamber. The following redox mediators were used at a concentration of 50 μM: quinhydrone ($E_{m,7} = +286$ mV); 2,6-dichlorophenolindophenol ($E_{m,7} = +217$ mV); thionine ($E_{m,7} = +60$ mV); phenazine ethosulfate ($E_{m,7} = +55$ mV); duroquinone ($E_{m,7} = +7$ mV); methylene blue ($E_{m,7} = -11$ mV); resorufin ($E_{m,7} = -50$ mV); indigodisulfonate ($E_{m,7} = -125$ mV); anthraquinone-2-sulfonic acid ($E_{m,7} = 225$ mV); phenosafranine ($E_{m,7} = -255$ mV); benzyl viologen ($E_{m,7} = -360$ mV); and methyl viologen ($E_{m,7} = -440$ mV). The redox potential was measured using a platinum measuring electrode with a calomel reference electrode, and the potential was adjusted with small additions of sodium dithionite and potassium ferricyanide solutions. After redox equilibration, samples were transferred to 3 mm internal diameter quartz EPR tubes and were rapidly frozen in liquid nitrogen.

Q-Pool Coupling Assay. The Q-pool coupling assay (Rothery & Weiner, 1991; Trieber *et al.*, 1994) was carried out as follows: (1) *Dithionite reduced samples.* 150 μL of membranes from *E. coli* DSS301 transformed with the plasmids used in this study were reduced with 5 mM dithionite for 2 min at 23 °C in an EPR tube prior to being rapidly frozen in liquid nitrogen. (2) *Dithionite reduced followed by treatment with DMSO*. Membranes were reduced with 5 mM dithionite for 2 min, and then DMSO was added to a concentration of 25 mM and the membranes were incubated for a further 2 min prior to being frozen. (3) *Dithionite reduced followed by treatment with fumarate*. Membranes were treated as in (2), but 25 mM fumarate was used instead of 25 mM DMSO.

Treatment of Membranes with HOQNO. For experiments carried out in the presence of HOQNO, a final concentration of 0.2 mM was used. Inhibitor was added from an ethanol solution, and equivalent volumes of ethanol were added to control samples.

EPR Spectroscopy. EPR spectra were recorded using a Bruker Spectrospin ESP-300 spectrometer equipped with an Oxford Instruments ESR-900 flowing helium cryostat. Instrument conditions and temperatures were as described in the individual figure legends. Spin quantitations were carried out by double integration as previously described (Cammack & Weiner, 1990). Two methods were employed to analyze redox titration data: (a) data were fitted to a multiple component redox model comprising independent redox components behaving as $n = 1$ species, and (b) data were fitted to a model describing the appearance of a doubly reduced 2[4Fe-4S] ferredoxin EPR signal (Mukund & Adams, 1990; Prince & Adams, 1987).

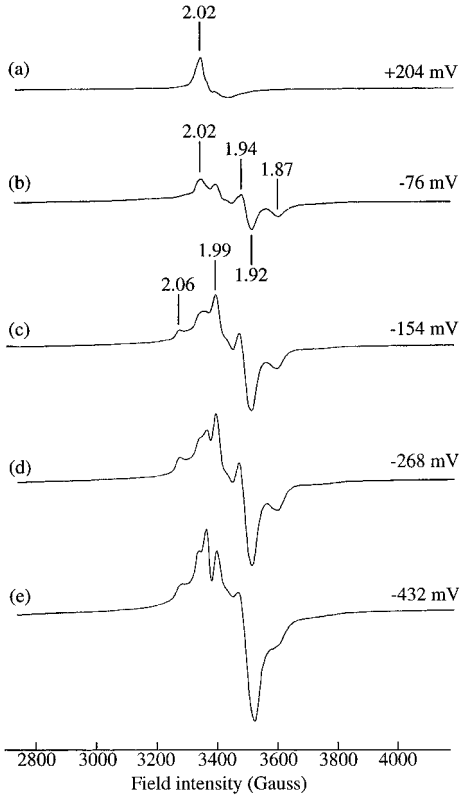

FIGURE 1: EPR spectra of redox poised membranes from a redox titration of F36/pDMS160 membranes. Samples were poised at the indicated potentials (E_h). Spectra were recorded under the following conditions: temperature, 12 K; microwave power, 20 mW; field modulation, 10 G_{pp} at 100 kHz.

RESULTS

Redox Potentiometry of the [4Fe-4S] Clusters of Wild-Type DmsABC. Figure 1 shows EPR spectra recorded at 12 K and at 20 mW microwave power of redox poised samples from a potentiometric titration of *E. coli* F36 membranes containing overexpressed wild-type DmsABC. *E. coli* F36 does not assemble a molybdenum cofactor into DmsA, so EPR spectra of membranes from this strain do not exhibit a low temperature spectrum of Mo(V) which arises from spin coupling between Mo(V) and at least one of the [4Fe-4S] clusters of DmsB (Cammack & Weiner, 1990). Figure 1a shows a spectrum of membranes poised at +204 mV. Noticeable in this spectrum is a sharp peak at $g = 2.02$ and a broad trough immediately upfield. These features are identical to those reported for the spectrum of the oxidized [3Fe-4S] (FR3) cluster of *E. coli* fumarate reductase (Frd-ABCD) (Johnson *et al.*, 1985b; Manadori *et al.*, 1992). As the redox potential is reduced to around −76 mV (Figure 1b), the spectrum of FR3 diminishes in intensity and a new species appears which has a spectrum comprising a peak at $g = 2.02$ (g_z), a peak-trough at $g = 1.94$ (g_y), and a trough at $g = 1.87$ (g_x). We have assigned this species to a rhombic EPR spectrum of the highest potential [4Fe-4S] cluster ligated by DmsB (Cammack & Weiner, 1990). As the potential is reduced to −154 mV (Figure 1c), a significant alteration takes place in the EPR line shape; peaks appear at $g = 2.06$ and $g = 1.99$, and the major features present at $E_h = -76$ mV increase in intensity. The change in line shape resulting in the appearance of the $g = 1.99$ and $g = 2.06$ features is similar to that observed in EPR spectra of 2[4Fe-4S] ferredoxins when these proteins change from containing a

single reduced [4Fe-4S] cluster to containing two reduced [4Fe-4S] clusters (Cammack *et al.*, 1994; Prince & Adams, 1987). Between $E_h = -154$ mV and $E_h = -268$ mV (Figure 1d), there is an increase in overall intensity of the EPR spectral features, but no significant change in the line shape. Between $E_h = -268$ mV and $E_h = -432$ mV (Figure 1e), there is a further increase in intensity accompanied by broadening of the $g = 2.06$ peak and the $g = 1.87$ trough. The overall line shape at -432 mV indicates that the spectrum arises from a complex interacting spin system comprising the four reduced [4Fe-4S] clusters of DmsB.

Figure 2 shows plots of the intensities of the various spectral features described above plotted as a function of redox potential (E_h). Figure 2a shows a plot of the intensity of the $g = 1.94$ peak-trough versus E_h. The data can be fitted to four redox components with $E_{m,7}$'s of -60, -122, -240, and -330 mV, in close agreement with those previously reported for the DmsABC [4Fe-4S] clusters (Cammack & Weiner, 1990). In order to further investigate the origin of the $g = 1.99$ peak that appears between approximately -50 and -150 mV, we plotted the intensity of this feature versus redox potential (Figure 2b). This feature reaches peak intensity at around $E_h = -200$ mV, and there is little further increase in its intensity with decreasing redox potential (Figure 1c−e and Figure 2b). The appearance of the $g = 1.99$ feature can be modeled as arising from a strong magnetic interaction between the $E_{m,7} = -60$ mV and the $E_{m,7} = -122$ mV [4Fe-4S] clusters, such as those found in the bacterial 2[4Fe-4S] cluster ferredoxins (Mukund & Adams, 1990; Prince & Adams, 1987). The data of Figure 2b were fitted in this manner to two interacting [4Fe-4S] clusters with $E_{m,7}$'s of -35 and -110 mV. These values are in reasonable agreement with the -60 and -122 mV midpoint potentials derived from fitting the intensity of the $g = 1.94$ peak-trough to independent redox couples (Figure 2a). Figure 2c shows the effect of redox potential on the relative spin intensities obtained from truncated double integrations of spectra recorded at 2 mW microwave power. In this case, the data are fitted to four independent redox components with $E_{m,7}$'s of -40, -110, -230 mV, and -360 mV. Overall, the data indicate that the four [4Fe-4S] clusters of DmsABC have $E_{m,7}$'s of -35 to -60 mV, -110 to -122 mV, -230 to -240 mV, and -330 to -360 mV.

Redox Potentiometry of the [4Fe-4S] Clusters and [3Fe-4S] Cluster of DmsAB^{C102S}C. Figure 3 shows EPR spectra recorded at 12 K and at 20 mW microwave power of redox poised samples from a potentiometric titration of F36 membranes containing overexpressed DmsAB^{C102S}C. Figure 3a shows a spectrum of membranes poised at +333 mV. Noticeable in this spectrum is a major peak at $g = 2.03$ with a major peak-trough immediately upfield. This is the spectrum of the [3Fe-4S] cluster assembled into DmsB^{C102} mutants in place of the [4Fe-4S] cluster ligated by Cys group III of the wild-type enzyme (Rothery & Weiner, 1991; Rothery & Weiner, 1993). As the E_h is decreased, the features of Figure 3a attributed to the [3Fe-4S] cluster disappear, and by +109 mV the spectrum is dominated by a peak at $g = 2.02$ with a broad trough immediately upfield. This spectrum is essentially identical to that of Figure 1a and can be attributed to the FR3 cluster of FrdABCD. Between approximately +109 and -64 mV (Figure 3b), the FR3 signal disappears and is replaced by a new species which has a peak at $g = 2.02$, a peak-trough at $g = 1.94$, and a

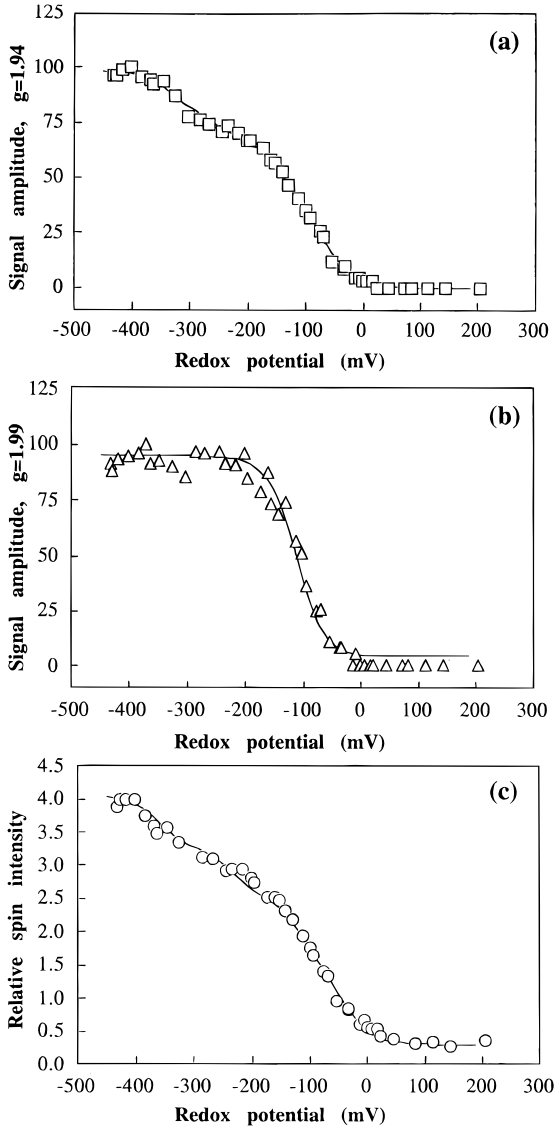

FIGURE 2: Potentiometric redox titration of the DmsABC [Fe-S] signals in *E. coli* F36 membranes. (a) Signal amplitude (% maximum) for the intensity of the $g = 1.94$ peak-trough versus E_h. Data were fitted to four independent $n = 1$ redox components with the following $E_{m,7}$'s and percent contributions: -60 mV (30%); -122 mV (35%); -240 mV (13%); -330 mV (20%). (b) Signal amplitude versus E_h for the appearance of the $g = 1.99$ peak versus E_h. Data were fitted to two redox components as described for the bacterial 2[4Fe-4S] ferredoxins (Mukund & Adams, 1990; Prince & Adams, 1987) such that the intensity of the $g = 1.99$ feature corresponds to the appearance of the spectrum of two magnetically coupled [4Fe-4S] clusters with $E_{m,7}$'s of -35 and -110 mV. (c) Relative spin intensity versus E_h. Data were fitted to four independent redox components with the following $E_{m,7}$'s and relative concentrations: -40 mV (1.1), -110 mV (1.1), -230 mV (0.75), and -360 mV (0.8). EPR spectra were recorded as described for Figure 1 for panels a and b. Spectra used to obtain the data in panel c were recorded at a microwave power of 2 mW.

shallow trough at $g = 1.87$. This spectrum is superficially similar to the spectrum of Figure 1b. However, spin quantitations suggest that this species contributes very little to the overall spin intensity of the fully reduced enzyme (Figure 3g, see below). Between -64 (Figure 3c) and -151 mV (Figure 3e), significant new features appear in the EPR spectrum comprising peaks at $g = 2.04$ and $g = 1.96$, and troughs at 1.89 and 1.87. The peak-trough at $g = 1.94$ also increases in intensity over this redox range. There is no appearance of a $g = 1.99$ peak as observed in membranes

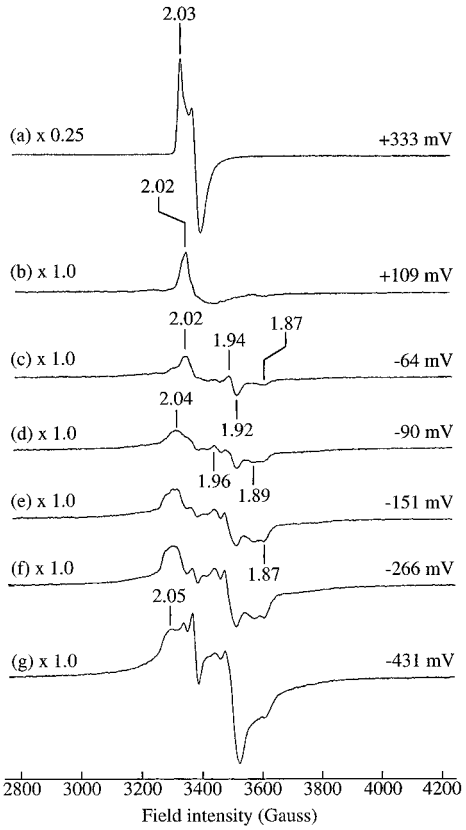

FIGURE 3: EPR spectra of redox poised membranes from a redox titration of F36/pDMS160-DmsB-C102S membranes. Samples were poised at the indicated potentials (E_h). Spectra were recorded as described for Figure 1.

containing wild-type DmsABC (Figure 1c), indicating that the spin-coupling from which this arises in the wild-type enzyme is lacking in DmsAB^{C102S}C. Between −151 (Figure 3e) and −266 mV (Figure 3f), the overall size of the spectral features increases, and this is accompanied by an apparent broadening of the signal as evidenced by the appearance of significant high and low field "tails" to the spectrum. Between −266 and −431 mV, the intensity of the spectrum increases with a loss of resolution of the $g = 1.89$ trough, and the $g = 2.04$ peak moves to $g = 2.05$.

Analyses of the differences between EPR spectra of potentiometrically poised samples from titrations of DmsABC and DmsAB^{C102S}C redox titrations are complicated by the interactions between the paramagnetic clusters present in the reduced enzymes. Redox titration data of the DmsB^{C102S} mutant was further analyzed by plotting the intensity of the $g = 1.94$ peak-trough versus redox potential (Figure 4a), the intensity of the $g = 2.04-2.05$ peak (Figure 4b), and the relative spin concentration of the samples versus redox potential (Figure 4c). The appearance of the $g = 1.94$ peak-trough can be fitted to three independent components with $E_{m,7}$'s of −45, −225, and −350 mV, suggesting that the component of the wild-type enzyme that is missing in the mutant is the $E_{m,7} = -120$ mV [4Fe-4S] cluster. However, closer examination of the spectra of Figure 3 suggest that analyses of the appearance of the $g = 1.94$ peak-trough are misleading, and that this feature is due to the reduction of the FrdABCD FR1 [2Fe-2S] cluster present in the F36 membranes used in this work. While this feature appears to maintain a relatively constant intensity between approximately −80 and −180 mV, it is clear from inspection

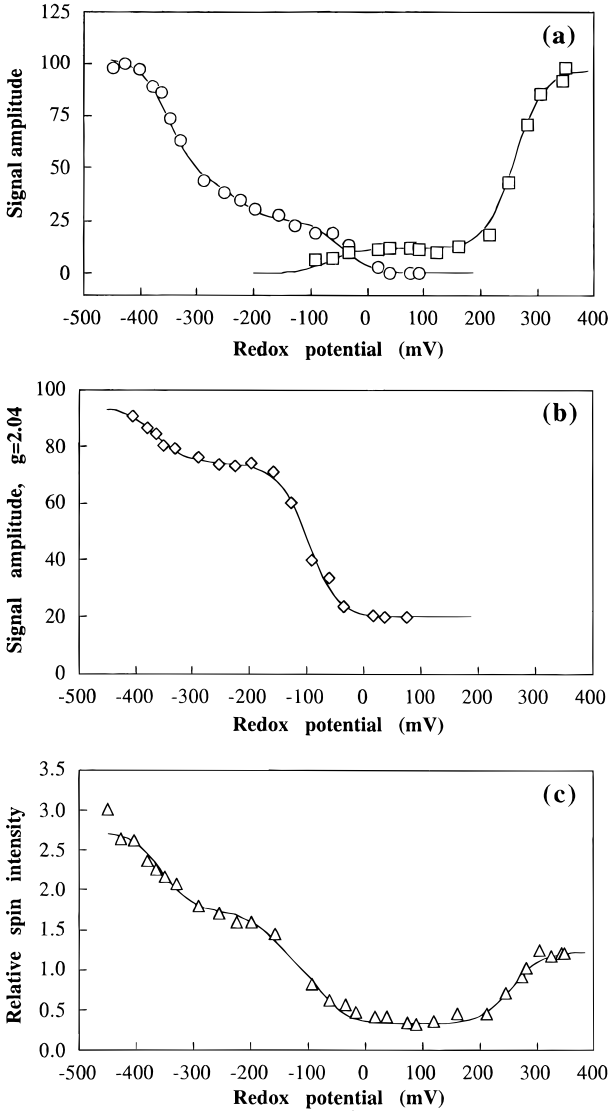

FIGURE 4: Potentiometric redox titration of the DmsAB^{C102S}C [Fe-S] signals in *E. coli* F36 membranes. (a) Signal amplitude (% maximum) of the $g = 1.94$ peak-trough (○) and [3Fe-4S] $g = 2.03$ peak (□) versus E_h. For the $g = 1.94$ feature, data were fitted to three independent redox components with $E_{m,7}$'s and percentage contributions of −45 mV (25%), −225 mV (17.5%), and −350 mV (60%). For the $g = 2.03$ feature, data were fitted to a major redox component with $E_{m,7} = +260$ mV. (b) Signal amplitude (% maximum) of the $g = 2.04-2.05$ peak versus E_h. Data were fitted to two independent redox components with $E_{m,7}$'s and percentage contributions of −100 mV (54%) and −365 mV (20%). (c) Relative spin intensity versus E_h. Data were fitted to four independent redox components with the following $E_{m,7}$'s and relative concentrations: +255 mV (0.9), −80 mV (0.8), −165 mV (0.6), and −355 mV (1.0). The $E_{m,7} = +255$ mV component corresponds to the [3Fe-4S] cluster. EPR spectra were recorded as described for Figure 1 for panel a. Spectra used to obtain the data in panel b were recorded at a microwave power of 2 mW.

of the spectra of Figure 3 that a major new species becomes reduced between $E_h = -64$ mV and −151 mV, with spectral features at $g = 2.04$ (peak) and $g = 1.96$ (peak) and 1.89 (trough). These features appear with an apparent $E_{m,7}$ of −100 mV (Figure 4b), and the overall line shape is quite distinct from that reported for the $E_{m,7} = -50$ mV [4Fe-4S] cluster of the DmsABC (cf. Figure 3d and Figure 1b). This is corroborated by analyses of the relative spin intensities of EPR spectra recorded at 12 K and 2 mW. Figure 4c shows the effect of E_h on the relative spin intensity of the DmsAB^{C102S}C spectrum, these data can be fitted to four redox

Table 2: Midpoint Potentials of Wild-Type and DmsB^{C102} Mutant DmsABC [Fe-S] Clusters

	$E_{m,7}$'s of $g = 1.94$ peak-trough[a]					$E_{m,7}$'s of relative spin intensity[b]				
enzyme	1	2	3	4	3Fe[c]	1[d]	2	3	4	3Fe
DmsABC	−60	−122	−240	−330		−40 (1.1)	−110 (1.1)	−230 (0.75)	−360 (0.8)	
DmsAB^{C102S}C		−45	−225	−350	+260		−80 (0.8)	−165 (0.6)	−355 (1.0)	255 (0.9)
DmsAB^{C102W}C		−10	−230	−340	+220		−90 (1.0)	−230 (0.75)	−375 (0.75)	200 (1.1)

a Data were obtained from spectra of F36 membranes recorded at 12 K and a microwave power of 20 mW. *b* Data were obtained from double integrations of spectra recorded at 12 K and at a microwave power of 2 mW. *c* The height of the $g = 2.03$ peak was measured in the [3Fe-4S] cluster redox titrations. *d* Numbers in parentheses indicate the estimated relative spin concentrations.

components with $E_{m,7}$'s of +255 mV ([3Fe-4S] cluster), −80, −165, and −355 mV ([4Fe-4S] clusters).

DmsAB^{C102W}C was also subjected to the same potentiometric analysis described for DmsAB^{C102S}C. The results of the potentiometric analyses of the two mutants and the wild-type enzyme are presented in Table 2. Overall, these indicate that in the DmsB^{C102} mutants, the [4Fe-4S] cluster of the wild-type enzyme which is converted into a [3Fe-4S] cluster in the DmsB^{C102} mutants is the $E_{m,7} = -50$ mV cluster.

Analyses of MQH_2/MQ Oxidation/Reduction Catalyzed by the DmsB^{C102} Mutants. DmsAB^{C102S}C and DmsAB^{C102W}C do not support respiratory growth on DMSO, and we have previously concluded that the effect of the mutations of DmsB^{C102} is to prevent MQH_2 oxidation and/or electron transfer through DmsB to the molybdenum cofactor of DmsA (Rothery & Weiner, 1991). One experimental technique that can be used to study the coupling of the [Fe-S] clusters of DmsB with the MQH_2 pool is the Q-pool coupling assay (Rothery & Weiner, 1991; Trieber *et al.*, 1994). This technique uses the distinctive EPR spectrum of *E. coli* FrdABCD as a probe of electron transfer in response to the addition of physiological substrates to dithionite reduced membranes. The *E. coli* strain used (DSS301) (Sambasivarao & Weiner, 1991) in these studies has a chromosomal deletion of the *dms* operon and also assembles a significant concentration of FrdABCD into the cytoplasmic membrane. Figure 5 shows EPR spectra recorded at 12 K of DSS301/pDMS160 membranes containing overexpressed DmsABC, showing the effects of dithionite reduction and subsequent additions of DMSO and fumarate. Figure 5a shows the spectrum of DSS301/pDMS160 membranes reduced with dithionite. Noticeable in this spectrum are peaks at $g = 2.05$, 2.02, 1.99, 1.96, and 1.94 as well as troughs at $g = 1.92$ and 1.88. The peak at $g = 2.02$ and the peak-trough at $g = 1.94$ can be attributed largely to the [2Fe-2S] FR1 cluster of FrdABCD (Trieber *et al.*, 1994; Werth *et al.*, 1990). The peaks at $g = 2.05$, 1.99, and 1.96, as well as the trough at $g = 1.88$, can be attributed to the spectrum of the DmsABC [Fe-S] clusters (Rothery & Weiner, 1991; Trieber *et al.*, 1994). Addition of DMSO (Figure 5b) or fumarate (Figure 5c) to dithionite reduced DSS301/pDMS160 membranes diminishes the features attributable to both the DmsABC and FrdABCD reduced [Fe-S] clusters with the concomitant appearance of the oxidized FR3 cluster spectrum. These data indicate that the redox states of the DmsABC and FrdABCD [Fe-S] clusters are coupled via the MQ pool, in agreement with our previous study (Rothery & Weiner, 1991). Figure 5d−f shows equivalent spectra for samples prepared in the presence of the MQH_2 analog HOQNO. In this case, addition of DMSO (Figure 5e) causes diminution of the features of the dithionite reduced spectrum of DmsABC but has little effect on the features attributed to FrdABCD.

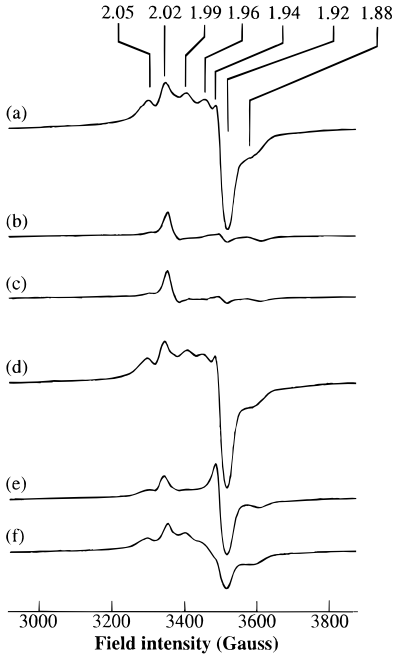

FIGURE 5: Q-pool coupling assay of DSS301 membranes containing overexpressed wild-type DmsABC. Spectra are of membranes from DSS301/pDMS160. (a) Dithionite reduced (5 mM). (b) Dithionite reduced (5 mM) and treated with 25 mM DMSO. (c) Dithionite reduced (5 mM) and treated with 25 mM fumarate. Spectra d−f are the same as spectra a−c, except that the samples contained 0.2 mM HOQNO. Dithionite reduced membranes were incubated under argon for 5 min at 23 °C prior to being frozen. Following addition of DMSO or fumarate, samples were incubated for a further 2 min. Spectra were recorded under the following conditions: temperature, 12 K; microwave power, 20 mW; modulation amplitude, 10 G_{pp} at 100 kHz. Spectra were corrected for protein concentration to a nominal 30 mg mL^{-1}.

Likewise, addition of fumarate (Figure 5f) causes diminution of the features attributable to FrdABCD, resulting in a spectrum containing the features attributable to the DmsABC [Fe-S] clusters (and a contribution from the partially oxidized FR3 cluster). These data indicate that HOQNO is able to block electron transfer between FrdABCD and DmsABC.

Figure 6 shows the results of a similar Q-pool coupling experiment performed with DSS301 membranes (DSS301/pDMS160-DmsB-C102S) containing overexpressed DmsAB^{C102S}C. The spectrum of dithionite reduced DSS301/pDMS160-DmsB-C102S membranes (Figure 6a) comprises peaks at $g = 2.05$, 2.02, 1.96, and 1.94 as well as troughs at $g = 1.92$ and $g = 1.88$. The peak at $g = 2.02$ and the peak-trough at $g = 1.94$ can again be attributed to the FR1 cluster of FrdABCD. The remaining features of the spectrum can be assigned to the reduced [4Fe-4S] clusters of DmsAB^{C102S}C, which has a significantly altered spectrum compared to the wild-type enzyme (Rothery & Weiner, 1991; Trieber *et al.*, 1994) (cf. Figure 1e and Figure 3g). Addition of DMSO

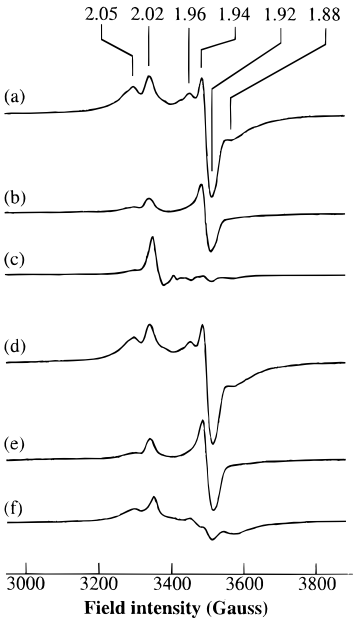

FIGURE 6: Q-pool coupling assay of DSS301 membranes containing overexpressed DmsAB^{C102S}C. Spectra were of samples prepared as described for Figure 5: (a−c) assay in absence of HOQNO; (d−f) assay in presence of 0.2 mM HOQNO.

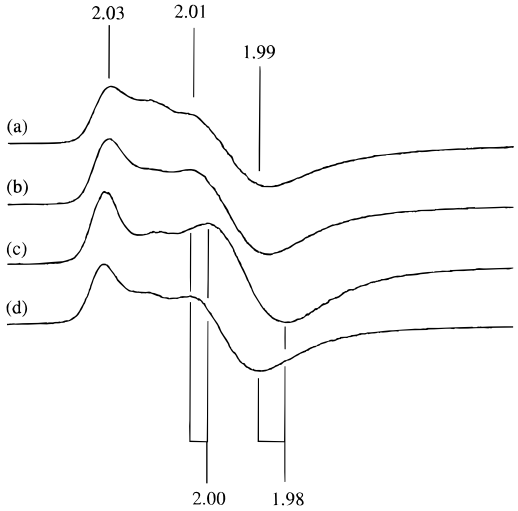

FIGURE 7: Effect of HOQNO on the [3Fe-4S] cluster line shape in DmsAB^{C102W}C and DmsAB^{C102S}C in HB101 membranes oxidized with 0.15 mM ferricyanide. The DmsAB^{C102W}C [3Fe-4S] cluster spectrum in the absence of (a) and in the presence of 0.2 mM HOQNO (b); the DmsAB^{C102S}C [3Fe-4S] cluster in the absence of (c) and in the presence of 0.2 mM HOQNO (d). Spectra were recorded as described for Figure 1 but with a narrower field scan width (500 G).

causes diminution of the DmsAB^{C102S}C spectrum (Figure 6b) but has little effect on the spectrum of the FrdABCD FR1 cluster, indicating that the DmsB^{C102} mutation blocks electron flow from MQH_2 to the [Fe-S] clusters of DmsB. Significantly, addition of fumarate to dithionite-reduced membranes containing DmsAB^{C102S}C causes diminution of *both* the FrdABCD spectrum (resulting in the appearance of the FR3 signal) *and* the DmsAB^{C102S}C spectrum (Figure 6c). This indicates that electron flow from MQH_2 to DmsB is blocked in the DmsB^{C102S} mutant but that electron flow in the opposite direction is not. When these experiments are repeated in the presence of HOQNO (Figure 6d−f), electron flow is blocked in both directions (cf. Figure 6c,f). Similar results were obtained by using the DmsB^{C102W} mutant (data not shown).

Interaction of a MQH_2 Binding Site with the [3Fe-4S] Cluster of the DmsB^{C102} Mutants. Three characteristics of the DmsB^{C102} mutant DmsABC led us to speculate that the $E_{m,7} = -50$ mV [4Fe-4S] cluster ligated primarily by Cys group III may be associated with an MQH_2 binding site of the holoenzyme: (i) in DmsAB^{C102S}C and DmsAB^{C102W}C the blockage of forward electron transfer detected using the Q-pool coupling assay affects all of the [Fe-S] clusters of DmsB, indicating that the $E_{m,7} = -50$ mV [4Fe-4S] cluster may be the point of entry for electrons passing from MQH_2 to the molybdenum cofactor of DmsA; (ii) the unidirectional electron transfer catalyzed by these mutants is consistent with a functional association of the $E_{m,7} = -50$ mV cluster with a MQH_2 binding site; and (iii) the $E_{m,7} = -50$ mV cluster appears to be thermodynamically competent to accept electrons directly from MQH_2 ($E_{m,7} = -70$ mV). We therefore studied the effect of the MQH_2 analog HOQNO on the EPR line shape of reduced DmsABC, DmsAB^{C102S}C, and DmsAB^{C102W}C. These studies were carried out using *E. coli* HB101, a strain which assembles high concentrations of plasmid encoded DmsABC into the cytoplasmic membrane (Rothery & Weiner, 1991; Trieber *et al.*, 1994). In dithionite-reduced HB101 membranes containing DmsABC, minor perturbations of the $g = 1.94$ peak-trough region were caused by the addition of HOQNO, and no significant effect could be detected in spectra of DmsAB^{C102S}C and DmsAB^{C102W}C in dithionite-reduced HB101 membranes (data not shown). Figure 7 shows EPR spectra recorded using a narrow (500 G) sweep width of oxidized DmsAB^{C102W}C and DmsAB^{C102S}C in HB101 membranes in the absence (Figure 7b,d) and presence (Figure 7a,c) of HOQNO. In DmsAB^{C102S}C, HOQNO elicits a significant change in the position of the $g = 2.01$ peak-trough, moving it to $g = 2.00$. The position of the $g = 2.03$ peak remains unaltered in the presence of HOQNO. Surprisingly, the effect of HOQNO on the [3Fe-4S] cluster line shape of the DmsB^{C102W} mutant is much reduced (Figure 7a), with only minor changes being detected in the $g = 2.01$ region.

In order to confirm that the observed changes in the EPR line shape of the DmsB^{C102S} cluster elicited by HOQNO are due to specific HOQNO binding to DmsABC and not due to a more general HOQNO induced effect on membrane structure, we carried out HOQNO binding titrations using HB101 membranes containing overexpressed DmsAB^{C102S}C (data not shown). The HOQNO effect was titratable and reached a maximum at around 20 μM in membranes containing approximately 15 μM DmsAB^{C102S}C (determined by quantitations of EPR spectra recorded at 12 K using 2 mW microwave power). No additional changes in the EPR spectrum were observed with increasing concentration, even at 2 mM HOQNO. However, due to the size of the shifts in the $g = 2.01-1.99$ peak trough region, it was not possible to accurately estimate the K_d for HOQNO binding to DmsAB^{C102S}C using the HOQNO binding titration data (data not shown).

The presence of DmsC has been shown to be necessary for MQH_2 binding and oxidation (Sambasivarao & Weiner, 1991), in a manner similar to that proposed for the anchor subunits of FrdABCD, FrdC and FrdD (Weiner *et al.*, 1986; Westenberg *et al.*, 1990). We have previously generated a mutant of FrdC (FrdC^{H82R}) which inhibits MQH_2 oxidation

Table 3: Enzyme Activities of Membranes Containing Amplified Levels of Wild-Type and Mutant DmsABC

enzyme	growth on GD[a]	Q-pool coupling[b]	$BV^{\bullet+}$:TMAO activity[c] DSS301	HB101
DmsABC	+	+	73	133
$DmsAB^{C102S}C$	−	−	76	112
$DmsAB^{C102W}C$	−	−	53	159
$DmsABC^{H65R}$	−	+/−	55	99
$DmsAB^{C102S}C^{H65R}$	−	−	68	148
$DmsAB^{C102W}C^{H65R}$	−	−	70	165

[a] Ability of the mutant enzymes to support growth with DMSO as respiratory oxidant. [b] Forward electron transfer from MQH_2 to DmsABC detected in the Q-pool coupling assay in DSS301 membranes. "+/−" indicates an incomplete inhibition detected with $DmsABC^{H65R}$. [c] Specific $BV^{\bullet+}$:TMAO oxidoreductase activities in units of μmol of $BV^{\bullet+}$ oxidized per mg of membrane protein per min.

by FrdABCD (Weiner *et al.*, 1986). Comparison of the sequence of DmsC with that of FrdC suggests that the equivalent residue in DmsC is H65. We therefore generated a $DmsC^{H65R}$ mutation and double mutants $DmsAB^{C102S}C^{H65R}$ and $DmsAB^{C102W}C^{H65R}$ to study the effect of the $DmsC^{H65R}$ mutation on the HOQNO induced [3Fe-4S] cluster line shape change. $DmsABC^{H65R}$ has a similar phenotype to that of $FrdABC^{H82R}D$. It is unable to support respiratory growth on DMSO, and it inhibits MQH_2 oxidation observed using the Q-pool coupling assay but retains considerable $BV^{\bullet+}$:TMAO oxidoreductase activity (Table 3). However, in contrast to the reported results with $FrdABC^{H82R}D$ (Weiner *et al.*, 1986), no stabilized radical species was observed by EPR (at 12 or 100 K) in the enzyme under turnover conditions in DSS301 membranes (data not shown). Comparison of spectra of reduced HB101 membranes containing $DmsAB^{C102S}C$, $DmsAB^{C102W}C$, $DmsAB^{C102S}C^{H65R}$, and $DmsAB^{C102W}C^{H65R}$ indicate that the $DmsC^{H65R}$ mutation has little effect on the concentration of the EPR detectable [4Fe-4S] clusters assembled into these mutant enzymes (data not shown).

Figure 8 shows the effect of the $DmsC^{H65R}$ mutation on the $DmsB^{C102S}$ and $DmsB^{C102W}$ [3Fe-4S] cluster EPR line shapes. Figure 8a,b shows the effect of HOQNO on the EPR line shape of oxidized $DmsAB^{C102S}C$. Figure 8c is the spectrum of HB101 membranes containing $DmsAB^{C102S}C^{H65R}$, and Figure 8d shows that the effect of HOQNO on the position of the $g = 2.01$ peak-trough is almost eliminated in this double mutant. Surprisingly, equivalent spectra of HB101 membranes containing $DmsAB^{C102W}C^{H65R}$ (Figure 8e,f) suggest that the $DmsC^{H65R}$ mutation has a direct effect on the environment of the $DmsB^{C102W}$ [3Fe-4S] cluster, resulting in a decrease in the intensity and broadening of its EPR signal. As with the $DmsAB^{C102S}C^{H65R}$ [3Fe-4S] spectrum, HOQNO has little effect on the $DmsAB^{C102W}C^{H65R}$ [3Fe-4S] EPR line shape.

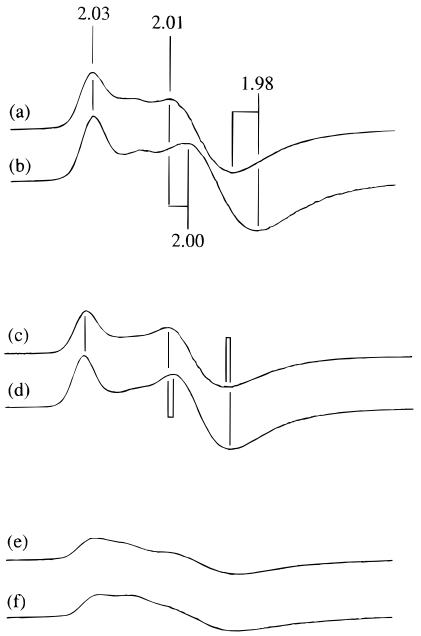

FIGURE 8: Effect of the $DmsC^{H65R}$ mutation on the HOQNO effect on the $DmsB^{C102S}$ and $DmsB^{C102W}$ [3Fe-4S] clusters. Spectra a and b are of HB101 membranes containing $DmsAB^{C102S}C$, in the absence of (a) and presence of (b) 0.2 mM HOQNO. Spectra c and d are of membranes containing $DmsAB^{C102S}C^{H65R}$ in the absence of (a) and presence of (b) 0.2 mM HOQNO. Spectra e and f are of membranes containing $DmsAB^{C102W}C^{H65R}$ in the absence of (a) and presence of (b) 0.2 mM HOQNO. EPR instrument conditions were as described for Figure 7. Samples were oxidized with 0.15 mM ferricyanide.

DISCUSSION

The results presented herein indicate that in the two mutants of DmsB, $DmsAB^{C102S}C$ and $DmsAB^{C102W}C$, the $E_{m,7} = -50$ mV [4Fe-4S] cluster ligated primarily by Cys group III of the wild-type enzyme is replaced by an $E_{m,7} = +220$ to +260 mV [3Fe-4S] cluster. We have also confirmed by EPR studies of the MQH_2 oxidoreductase activities of $DmsAB^{C102S}C$ and $DmsAB^{C102W}C$, and the effect of HOQNO on these mutant enzymes, that the [3Fe-4S] clusters are functionally and conformationally linked to a MQH_2 (HOQNO) binding site of DmsC. The data indicate that $DmsC^{H65R}$ may be a component of this site. By extrapolation, we conclude that the $E_{m,7} = -50$ mV cluster of the wild-type enzyme is also functionally and conformationally linked to this MQH_2 binding site and is an important component of the electron transfer pathway through DmsB to the molybdenum cofactor of DmsA. This is further supported by the thermodynamic competency of the $E_{m,7} = -50$ mV cluster of DmsABC to accept electrons from MQH_2 ($E_{m,7} = -70$ mV). These conclusions are also consistent with topographical data which suggests that the $DmsB^{C102S}$ [3Fe-4S] cluster (and the $E_{m,7} = -50$ mV cluster of the wild-type enzyme) is located approximately 21 Å from the cytoplasmic side surface of $DmsAB^{C102S}C$ and close to the cytoplasmic-side membrane interface (Rothery & Weiner, 1993), a position consistent with a role for the $E_{m,7} = -50$ mV [4Fe-4S] cluster in electron transfer from a MQH_2 binding site located in DmsC.

Models for the interaction of ferredoxin-like Cys groups with [4Fe-4S] clusters indicate that the first three Cys residues (C_A−C_C) provide three ligands to one cluster, while the fourth Cys residue (C_D) provides the fourth ligand to a second [4Fe-4S] or [3Fe-4S] cluster with which the Cys group is structurally paired (Bruschi & Guerlesquin, 1988; Moura *et al.*, 1994). In the bacterial 2[4Fe-4S] ferredoxins the two [4Fe-4S] clusters exhibit strong spin−spin interactions, resulting in a major difference between the line shape of the EPR spectrum of the singly reduced protein and that of the doubly reduced protein (Prince & Adams, 1987). The EPR spectrum of DmsABC undergoes a major change in line shape between the singly reduced state ($E_h < \sim -50$ mV) and the doubly reduced state ($E_h < \sim -120$ mV) as

illustrated in Figure 1. The redox behavior of the two highest potential [4Fe-4S] clusters of DmsABC can be modeled as that of two interacting clusters in a 2[4Fe-4S] ferredoxin-like motif within DmsB (Figure 2b). We can therefore conclude, on the basis of the sequence homologies between the Cys groups of DmsB and those of the well characterized bacterial 2[4Fe-4S] ferredoxins and the potentiometric behavior of DmsABC followed by EPR, that the $E_{m,7} = -50$ mV and $E_{m,7} = -120$ mV [4Fe-4S] clusters comprise a 2[4Fe-4S] ferredoxin-like motif within DmsB. As the E_h is reduced below −120 mV and the two low potential clusters of DmsABC become reduced, it is not possible to determine if there are similar interactions between $E_{m,7} = -240$ mV and the $E_{m,7} = -330$ mV [4Fe-4S] clusters. This is largely due to the overall complexity of the EPR spectrum of the multiply reduced enzyme, which arises from the four interacting reduced [4Fe-4S] clusters.

EPR spectra of potentiometrically poised F36 membranes containing overexpressed DmsAB^{C102S}C indicate that the conversion of one of the [4Fe-4S] clusters of the wild-type enzyme to a [3Fe-4S] cluster results in the loss of the $g = 1.99$ spectral feature which we have assigned to the spin−spin interaction between the $E_{m,7} = -50$ mV and $E_{m,7} = -120$ mV [4Fe-4S] clusters. This suggests that the [4Fe-4S] cluster of DmsABC which is converted to a [3Fe-4S] cluster in DmsAB^{C102S}C corresponds to one of the two highest potential clusters. Careful analyses of the line shape changes in the spectra of Figure 3, the effect of E_h on the appearance of the $g = 2.04-2.05$ peak (Figure 4b), and the relative spin concentration (Figure 4c) indicate that the [4Fe-4S] cluster that is missing in the DmsB^{C102S} mutant is the $E_{m,7} = -50$ mV cluster. Given that the overall changes imposed on the structure of DmsB by the change in cluster type ligated by Cys group III from a [4Fe-4S] cluster to a [3Fe-4S] cluster should be relatively minor (compared to, for example, the total loss of the cluster), we have assigned Cys group III as providing three ligands to the $E_{m,7} = -50$ mV [4Fe-4S] cluster. This assignment has important implications for the assignment of the other Cys groups to the three remaining potentiometrically identified [4Fe-4S] clusters of DmsABC. A model for the interaction of the polypeptide chain with the four [4Fe-4S] clusters has been proposed in which Cys groups I/II and III/IV comprise two 2[4Fe-4S] ferredoxin motifs (Weiner *et al.*, 1992). This could arise evolutionarily as the result of a gene duplication event and would result in the assignment of Cys group IV as providing three ligands to the $E_{m,7} = -120$ mV [4Fe-4S] cluster. However, consideration of the spacing of the Cys groups and comparisons with the large number of sequences available for bacterial 2[4Fe-4S] ferredoxins suggests a second possible model. This would arise evolutionarily from a gene insertion event, resulting in a protein in which Cys groups II/III comprise an 2[4Fe-4S] ferredoxin motif which has been inserted into a similar motif comprising Cys groups I/IV. This would result in the assignment of Cys group II as providing three ligands to the $E_{m,7} = -120$ mV [4Fe-4S] cluster of the wild-type enzyme. However, by generating a number of site-directed mutants of other Cys residues in DmsB, we have been unable to obtain enough mutants which express well and assemble to high concentrations in the cytoplasmic membrane to be able to generate a comprehensive assignment of the four Cys groups to the four potentiometrically identified [4Fe-4S] clusters (R.A. Rothery and J. H. Weiner, unpublished results). Further studies are in progress to achieve this aim.

Our assignment of the $E_{m,7} = -50$ mV cluster to Cys group III bears interesting comparison with studies of *E. coli* nitrate reductase NarGHI. NarH contains three [4Fe-4S] clusters (Guigliarelli *et al.*, 1992) and one [3Fe-4S] cluster (Johnson *et al.*, 1985a) with $E_{m,8.3}$'s of +60 ([3Fe-4S] cluster), +80, −200, and −400 mV ([4Fe-4S] clusters). Mutations of the NarH Cys group I result in the loss of the $E_{m,8.3} = +80$ mV [4Fe-4S] cluster (Augier *et al.*, 1993a), the highest potential cluster of the enzyme, whereas, in DmsB, mutations of Cys group III (DmsB^{C102}) result in loss of the highest potential cluster. However, there are a number of differences between the DmsB and NarH which may explain this difference in the apparent ligation of the highest potential clusters. First, NarH is relatively large compared to DmsB (NarH, 512 aa; DmsB, 207 aa), and the spacings between its Cys groups are somewhat different (Blasco *et al.*, 1989). Secondly, studies of NarGHI have been carried out on purified preparations of the NarGH dimer which lacks the NarI membrane anchor and cytochrome subunit (Augier *et al.*, 1993a,b; Guigliarelli *et al.*, 1992), whereas our work on DmsB has been performed on the membrane-bound DmsABC holoenzyme. Thirdly, the membrane anchor subunit of NarGHI, NarI, is a cytochrome (Chaudhry & MacGregor, 1983). Consequently, the electron transfer through the [Fe-S] clusters of NarH may not follow an equivalent route to that through DmsB, resulting in a different overall pattern of $E_{m,7}$'s in the [Fe-S] clusters of the two enzymes.

The conversion of the [4Fe-4S] cluster ligated by Cys group III of DmsB of the wild-type enzyme to a [3Fe-4S] cluster changes the $E_{m,7}$ of the cluster ligated by C102 from −60 mV to between +220 and +260 mV, a change of between 280 and 320 mV. In FrdABCD the FR3 cluster has been converted to a [4Fe-4S] cluster by generating a FrdB^{V207C} mutant (Manadori *et al.*, 1992). In this case the $E_{m,7} = -70$ mV [3Fe-4S] cluster is changed into an $E_{m,7} = -350$ mV [4Fe-4S] cluster, a change in $E_{m,7}$ of 280 mV between the two cluster types. In the DmsB^{C102} mutants there is a difference in $E_{m,7}$ of around 40 mV between the [3Fe-4S] cluster with a Trp and Ser at the C_B position. This suggests that the nature of the residue at the C_B position of the [3Fe-4S] cluster ligating Cys groups may play a role in defining the $E_{m,7}$ of the cluster.

We have used the Q-pool coupling assay (Rothery & Weiner, 1991; Trieber *et al.*, 1994) to re-evaluate the effect of the DmsB^{C102S} and DmsB^{C102W} mutations on the electron transfer between DmsABC and the MQH_2 pool. It is clear from the data of Figure 6 that in DmsAB^{C102S}C electron transfer is blocked in the physiologically forward direction (from MQH_2 to DmsA), whereas electron transfer in the reverse direction is still possible. There are a number of possible explanations for the unidirectional electron transfer catalyzed by the DmsB^{C102} mutants of DmsABC:

(1) The change of cluster type ligated by DmsB^{C102} causes perturbation of the MQH_2 binding site with which it is associated, resulting in a change in the relative affinities of the site for MQH_2 versus menaquinone (MQ). The affinity of the DmsB^{C102} mutant enzymes could have a negligible affinity for MQH_2 compared to MQ, resulting in essentially complete inhibition of MQH_2 oxidation in response to the addition of DMSO.

(2) DmsABC may possess more than one MQH_2 site, one of which has a high affinity for MQ, and the other having high affinity for MQH_2. In the $DmsB^{C102}$ mutants electron transfer from the MQH_2 binding site would be disrupted, while electron transfer to the MQ binding site would not. This explanation bears interesting comparison with a number of other enzyme systems. Structural and kinetic studies of the bacterial photoreaction center have clearly shown that this complex contains two quinone binding sites, the Q_A and Q_B sites (Ermler *et al.*, 1994; Okamura & Feher, 1992), the Q_A site has a tightly bound quinone and functions to transfer electrons to the Q_B site which is in dynamic equilibrium with the quinone pool. Similar Q_A/Q_B binding sites have been proposed for *E. coli* FrdABCD (Westenberg *et al.*, 1990, 1993), but, in this case, the function of the Q_A site is proposed to be the reduction of MQ (or quinone analogs) and function of the Q_B site is proposed to be the oxidation of MQH_2 (or quinol analogs). Mitochondrial complex III (cytochrome bc_1) also contains two quinol/quinone binding sites which are central to the mechanism of the protonmotive Q-cycle (Q_i and Q_o) (Trumpower, 1990). Potentiometrically poised mitochondrial complex II (succinate:ubiquinol oxidoreductase) has been shown to contain two interacting semiquinol radicals (Ruzicka *et al.*, 1975; Salerno & Ohnishi, 1980). In *E. coli* cytochrome *bo*, two quinone binding sites have been identified, the Q_H and the Q_L sites, Q_H being a high-affinity binding site and Q_L being a low-affinity binding site (Sato-Watanabe *et al.*, 1994). Thus, a common theme is emerging for quinol oxidation via two binding sites in many of these oxidoreductases, and it is possible that DmsABC also contains two such sites.

The effect of the MQH_2 analog HOQNO on the EPR line shape of the $DmsB^{C102S}$ [3Fe-4S] cluster is good evidence that the cluster (and by extrapolation, the $E_{m,7} = -50$ mV [4Fe-4S] cluster of the wild-type enzyme) is conformationally and functionally linked to a MQH_2 binding site. The different behavior of the $DmsB^{C102S}$ and $DmsB^{C102W}$ mutants with respect to HOQNO binding is further evidence for this. The Trp side chain appears to be sufficiently bulky to interfere with the HOQNO effect of the [3Fe-4S] cluster line shape. The effect of HOQNO on the $DmsB^{C102S}$ [3Fe-4S] cluster line shape is reminiscent of the effect of a number of respiratory chain inhibitors on the EPR line shape of the Rieske [2Fe-2S] cluster of mitochondrial cytochrome bc_1 (Trumpower, 1990; von Jagow & Ohnishi, 1985). The role of the Rieske center is to accept one electron from the oxidation of ubiquinol at the Q_o site of this enzyme (the other electron is transferred to one of the hemes, b_o). It is possible to speculate that a broadly similar role can be assigned to the $E_{m,7} = -50$ mV [4Fe-4S] cluster of wild-type DmsABC; electron transfer through DmsB would start at this cluster. It has previously been shown by complementation analyses (Sambasivarao & Weiner, 1991) that DmsC is necessary for MQH_2 binding and oxidation by DmsABC. To further these studies, we generated a mutant in DmsC, $DmsC^{H65R}$, in which physiological MQH_2 oxidation is inhibited. By generating $DmsB^{C102S}$ and $DmsB^{C102W}$ double mutants with $DmsC^{H65R}$, we have been able to explore the interaction between the region around $DmsC^{H65R}$ and the mutant [3Fe-4S] cluster of DmsB. The $DmsC^{H65R}$ mutation appears to almost abolish the HOQNO effect on the [3Fe-4S] cluster line shape $g = 2.01$ peak-trough, suggesting that the $DmsC^{H65R}$ mutation interferes with HOQNO binding at a quinol binding site associated with this His residue, or that the conformational link between the MQH_2 binding site and the [3Fe-4S] cluster is disrupted by the $DmsC^{H65R}$ mutation. The effect of the $DmsC^{H65R}$ mutation on the line shape of the $DmsB^{C102W}$ [3Fe-4S] cluster suggests that $DmsB^{C102}$ and $DmsC^{H65}$ are in close proximity in the holoenzyme.

Our conclusion that the $E_{m,7} = -50$ mV cluster ligated by Cys group III of DmsABC has an important role in MQH_2 oxidation bears interesting comparison with results obtained using mutants of FrdABCD. By generating a mutant of the $E_{m,7} = -70$ mV [3Fe-4S] FR3 cluster binding domain of FrdB ($FrdB^{P159Q}$), Cecchini and co-workers (Cecchini *et al.*, 1995) were able to show an apparent hydroxyl radical dependent inactivation of FrdABCD under aerobic conditions which was alleviated by HOQNO. These workers proposed that a close FR3 cluster−MQH_2 binding site interaction is responsible for the aerobic generation of hydroxyl radicals by $FrdAB^{P159Q}CD$. It is also notable that the [3Fe-4S] to [4Fe-4S] cluster conversion elicited by the $FrdB^{V207C}$ mutant also led to a significant decrease in the ability of $FrdAB^{V207C}$-CD to transfer electrons to and from quinol analogs (Manadori *et al.*, 1992). Given these results with FrdABCD, it is perhaps not surprising that in DmsABC there is an interaction between a MQH_2 binding site and the [4Fe-4S] cluster most thermodynamically appropriate to accept electrons from this quinol.

The transmembrane topology of DmsC has recently been studied using a combination of *blaM* and *phoA* gene fusions (Sambasivarao *et al.*, 1990; Weiner *et al.*, 1993), and it has been proposed that DmsC forms eight transmembrane helices across the cytoplasmic membrane. In the proposed topology, $DmsC^{H65}$ is placed close to the periplasmic surface of the cytoplasmic membrane. We have previously shown that the [3Fe-4S] cluster of the $DmsB^{C102S}$ mutant is located approximately 21 Å below the cytoplasmic side surface of $DmsAB^{C102S}C$, approximately parallel with the membrane surface level (Rothery & Weiner, 1993). EPR studies of the DmsAB and $DmsAB^{C102S}$ dimer indicated that the [3Fe-4S] cluster of the $DmsB^{C102S}$ mutant either is not assembled into the dimer or is extremely labile. These results indicated that the $DmsB^{C102S}$ [3Fe-4S] cluster is located near the inside edge of the membrane extrinsic DmsAB dimer. Thus, there is an apparent conflict between the location of $DmsC^{H65}$ determined from EPR studies of the intact holoenzyme and its location determined from gene fusion experiments which destroy the overall structure of the holoenzyme. It is possible that the membrane-spanning part of transmembrane helix II (which bears the $DmsC^{H65}$ residue) may have to be adjusted in the model of DmsC (Weiner *et al.*, 1993) to move the position of this residue closer to the cytoplasmic side surface of the model. There is a large periplasmic loop after $DmsC^{H65}$ in the model which could accommodate modifications to make it more consistent with the biophysical data. Alternatively, it is possible that the introduction of the positively charged Arg may affect the assembly of helix II into the membrane. However, we believe that this latter explanation is unlikely to be valid, as it would have severe implications for the insertion and potential orientations of the other transmembrane helices of DmsC, which would presumably have a negative effect on the association of DmsAB with DmsC.

Overall, the data presented herein indicates the importance of the $E_{m,7} = -50$ mV [4Fe-4S] cluster of DmsB in

mediating electron transfer from MQH_2 to DMSO. We have shown that mutants of $DmsB^{C102}$ in which this cluster is replaced by a [3Fe-4S] catalyze unidirectional electron transfer from DmsB to MQ. The $DmsB^{C102}$ mutant [3Fe-4S] cluster appears to be conformationally and perhaps spatially linked to a MQH_2 binding site of the holoenzyme. These results represent an important step in delineating the physiological electron transfer pathway through DmsABC.

ACKNOWLEDGMENT

Thanks are due to Richard Cammack for critical reading of the manuscript.

REFERENCES

Augier, V., Asso, M., Guigliarelli, B., More, C., Bertrand, P., Santini, C., Blasco, F., Chippaux, M., & Giordano, G. (1993a) *Biochemistry 32*, 5099−5108.

Augier, V., Guigliarelli, B., Asso, M., Bertrand, P., Frixon, C., Giordano, G., Chippaux, M., & Blasco, F. (1993b) *Biochemistry 32*, 2013−2023.

Berg, B. L., Li, J., Heider, J., & Stewart, V. (1991) *J. Biol. Chem. 266*, 22380−22385.

Bilous, P. T., & Weiner, J. H. (1985) *J. Bacteriol. 162*, 1151−1155.

Bilous, P. T., & Weiner, J. H. (1988) *J. Bacteriol. 170*, 1511−1518.

Bilous, P. T., Cole, S. T., Anderson, W. F., & Weiner, J. H. (1988) *Mol. Microbiol. 2*, 785−795.

Blasco, F., Iobbi, C., Giordano, G., Chippaux, M., & Bonnefoy, V. (1989) *Mol. Gen. Genet. 218*, 249−256.

Blasco, F., Iobbi, C., Ratouchniak, J., Bonnefoy, V., & Chippaux, M. (1990) *Mol. Gen. Genet. 222*, 104−111.

Bruschi, M., & Guerlesquin, F. (1988) *FEMS Microbiol. Rev. 54*, 155−176.

Cammack, R., & Weiner, J. H. (1990) *Biochemistry 29*, 8410−8416.

Cammack, R., Williams, R., Guigliarelli, B., More, C., & Bertrand, P. (1994) *Biochem. Soc. Trans. 22*, 721−725.

Cecchini, G., Sices, H., Schröder, I., & Gunsalus, R. P. (1995) *J. Bacteriol. 177*, 4587−4592.

Chamorovsky, S. K., & Cammack, R. (1982) *Photobiochem. Photobiophys. 4*, 195−200.

Chaudhry, G. R., & MacGregor, C. H. (1983) *J. Biol. Chem. 258*, 5819−5827.

Condon, C., & Weiner, J. H. (1988) *Mol. Microbiol. 2*, 43−52.

Ding, H., Robertson, D. E., Daldal, F., & Dutton, P. L. (1992) *Biochemistry 31*, 3144−3158.

Dutton, P. L. (1978) *Methods Enzymol. 54*, 411−435.

Ermler, U., Michel, H., & Schiffer, M. (1994) *J. Bioenerg. Biomembr. 26*, 5−15.

Guigliarelli, B., Asso, M., More, C., Augier, V., Blasco, F., Pommier, J., Giordano, G., & Bertrand, P. (1992) *Eur. J. Biochem. 207*, 61−68.

Hägerhäll, C., Sled, V., Hederstedt, L., & Ohnishi, T. (1995) *Biochim. Biophys. Acta. 1229*, 356−362.

Johnson, M. K., Bennett, D. E., Morningstar, J. E., Adams, M. W. W., & Mortenson, L. E. (1985a) *J. Biol. Chem. 260*, 5456−5463.

Johnson, M. K., Morningstar, J. E., Cecchini, G., & Ackrell, B. A. C. (1985b) *Biochem. Biophys. Res. Commun. 131*, 653−658.

Krafft, T., Bokranz, M. O. K., Schröder, I., Fahrenholz, F., Kojro, E., & Kröger, A. (1992) *Eur. J. Biochem. 206*, 5456−5463.

Manadori, A., Cecchini, G., Shröder, I., Gunsalus, R. P., Werth, M. T., & Johnson, M. K. (1992) *Biochemistry 31*, 2703−2712.

Moura, J. J. G., Macedo, A. L., & Palma, P. N. (1994) *Methods Enzymol. 243*, 165−188.

Mukund, S., & Adams, M. W. W. (1990) *J. Biol. Chem. 265*, 11508−11516.

Ohnishi, T., Sled, V. D., Rudninsky, N. I., Meinhardt, S. W., Yagi, T., Hatefi, Y., Link, T., von Jagow, G., Saribas, A. S., & Daldal, F. (1994) *Biochem. Soc. Trans. 22*, 191−197.

Okamura, M. Y., & Feher, G. (1992) *Annu. Rev. Biochem. 61*, 861−896.

Prince, R. C., & Adams, M. W. W. (1987) *J. Biol. Chem. 262*, 5125−5128.

Robertson, D. E., Daldal, F., & Dutton, P. L. (1990) *Biochemistry 29*, 11249−11260.

Rothery, R. A., & Weiner, J. H. (1991) *Biochemistry 30*, 8296−8305.

Rothery, R. A., & Weiner, J. H. (1993) *Biochemistry 32*, 5855−5861.

Ruzicka, F. J., Beinert, H., Schlepler, K. L., Dunham, W. R., & Sands, R. H. (1975) *Proc. Natl. Acad. Sci. U.S.A. 72*, 2886−2890.

Salerno, J. C., & Ohnishi, T. (1980) *Biochem. J. 192*, 769−781.

Sambasivarao, D., & Weiner, J. H. (1991) *J. Bacteriol. 173*, 5935−5943.

Sambasivarao, D., Scraba, D. G., Trieber, C. A., & Weiner, J. H. (1990) *J. Bacteriol. 172*, 5938−5948.

Sambrook, J., Fritsch, E. F., & Maniatis, T. (1989) *Molecular Cloning: A Laboratory Manual*, 2nd ed., Cold Spring Harbor Laboratory Press, Cold Spring Harbor, NY.

Sato-Watanabe, M., Mogi, T., Ogura, T., Kitagawa, T., Myoshi, H., Iwamura, H., & Anraku, Y. (1994) *J. Biol. Chem. 269*, 28908−28912.

Smirnova, I. A., Hägerhäll, C., Konstantinov, A. A., & Hederstedt, L. (1995) *FEBS Lett. 359*, 23−26.

Trieber, C. A., Rothery, R. A., & Weiner, J. H. (1994) *J. Biol. Chem. 269*, 7103−7109.

Trumpower, B. L. (1990) *Microbiol. Rev. 54*, 101−129.

von Jagow, G., & Ohnishi, T. (1985) *FEBS Lett. 185*, 311−315.

Warren, P. V., Smart, L. B., McIntosh, L., & Golbeck, J. H. (1993) *Biochemistry 32*, 4411−4419.

Weiner, J. H., Cammack, R., Cole, S. T., Condon, C., Honoré, N., Lemire, B. D., & Shaw, G. (1986) *Proc. Natl. Acad. Sci. U.S.A. 83*, 2056−2060.

Weiner, J. H., MacIsaac, D. P., Bishop, R. E., & Bilous, P. T. (1988) *J. Bacteriol. 170*, 1505−1510.

Weiner, J. H., Rothery, R. A., Sambasivarao, D., & Trieber, C. A. (1992) *Biochim. Biophys. Acta 1102*, 1−18.

Weiner, J. H., Shaw, G., Turner, R. J., & Trieber, C. A. (1993) *J. Biol. Chem. 268*, 3238−3244.

Werth, M. T., Cecchini, G., Manodori, A., Ackrell, B. A. C., Schröder, I., Gunsalus, R. P., & Johnson, M. K. (1990) *Proc. Natl. Acad. Sci. U.S.A. 87*, 8965−8969.

Westenberg, D. J., Gunsalus, R. P., Ackrell, B. A. C., & Ceccini, G. (1990) *J. Biol. Chem. 265*, 19560−19567.

Westenberg, D. J., Gunsalus, R. P., Ackrell, B. A. C., Sices, H., & Cecchini, G. (1993) *J. Biol. Chem. 268*, 815−822.

Zhao, J., Li., N., Warren, P. V., Golbeck, J. H., & Bryant, D. A. (1992) *Biochemistry 31*, 5093−5099.

BI951584Y